Radiation and Particle Therapy

A. Bocci
DITANET Experienced Researcher, National Accelerator Centre (CNA), 41092 Seville, Spain.

Z. Abou-Haïdar and M. A. G. Alvarez
National Accelerator Centre (CNA), 41092 Seville, Spain.

M. A. Cortés-Giraldo, M. I. Gallardo, J. M. Espino, and J. M. Quesada
Department of Atomic, Molecular and Nuclear Physics (FAMN), University of Seville, 41012 Seville, Spain.

R. Arráns
Virgen Macarena University Hospital, 41009 Seville, Spain.

A. Pérez Vega-Leal
School of Engineering, University of Seville, 41092 Seville, Spain.

F. J. Pérez Nieto
Instalaciones Inabensa S.A., 41007 Seville, Spain.
(Dated: May 2, 2012)

Following the main objectives of DITANET to develop new techniques for future particle accelerators and based on the background of National Accelerator Centre (CNA) in nuclear reactions and instruments, our research project was oriented to radiation and particle therapy. As Experienced Researcher (ER), supported by DITANET, a novel treatment verification system for Intensity Modulated Radiation Therapy (IMRT) was developed. The project was to characterize an experimental set-up based on a silicon DC-coupled single-sided strip detector (SSSSD) used to validate a 2D dosimetric system for axial plane measurements. Such a method is in the process of being patented and it is also being improved in order to offer an accurate system for on-line IMRT treatment verification in an hospital. Moreover a second project was based on the European collaboration dedicated to study different ions fragmentation cross sections for accurate treatment planning for particle therapy. In this experiment named FIRST: Fragmentation of Ions Relevant for Space and Therapy, the main activity was to work on beam tracking reconstruction software of the experimental data of a drift chamber used to measure the beam trajectory and the impact point on a target with a spatial resolution of 100 μm.

I. INTRODUCTION

Radiation and particle therapy are nowadays a well established and a rapidly expanding technique, respectively, used in the treatment of tumors. As treatments are evolving and increasing in terms of complexity, a parallel development is required for dosimetric treatment verifications [1]. A common technique, although not simple, is the Intensity Modulated Radiation Therapy (IMRT) that uses a linac equipped with a multileaf collimator (MLC) [2, 3].

Dose distribution verification is highly advisable prior to real dose delivery to the patient in complex radiotherapy treatments, as Treatment Planning Systems (TPS) might miscalculate, under some circumstances, the dose delivered to the patient [4, 5].

Radiographic films are used for IMRT Quality Assurance (QA) and for planned treatments verification [2, 6]. The main drawback of radiometric film is the reading process that makes it unsuitable as an on-line detector. Therefore, it is necessary to develop new detection systems that enhance the traditional ones, and that are able to verify in a simple and accurate way complex treatment plannings.

Recently, 2D arrays based on silicon diodes and ionization chambers have been developed and used as on-line detectors. Such systems have the advantage over films that they can provide a real-time dose. However, the spatial resolution of commercial 2D arrays is still far from what is needed in treatment verification when compared to film dosimetry [7–9]. Spatial resolution of 2D arrays is still poor (cm or some mm), they require complex electronics and their design approach is still limited to dose maps in coronal planes.

Many efforts have been done to develop silicon detectors for medical physics applications, taking advantage of the experience earned in detector technology from high energy physics research (i.e., on silicon tracking detectors and data acquisition systems) [10]. In particular, research is oriented towards silicon microstrip technology to improve spatial resolution in radiotherapy treatment verification [11, 12]. Pixelated silicon array detectors were also developed, such as in the framework of the European project MAESTRO [13]. To obtain submillimetric spatial resolutions, these devices require a high number of allocated channels and a complex multichannel read-

out electronics based on application-specific integrated circuits (ASICs) [11, 13–15].

Following, we present the characterization of a silicon DC-coupled single-sided strip detector (SSSSD) from Micron semiconductors Ltd. irradiated with a Linac at 6-MV photon mode. Two phantoms prototypes have been designed for the detector characterization and treatment verification: a water-equivalent slab phantom with the detector placed perpendicularly to the beam direction and a quasi-anthropomorphic cylindrical phantom with the capability of rotating along its symmetry axis. Since common ways to present dose distributions is a dose map in the patient axial plane, as an innovation the detector in the cylindrical phantom was placed parallel to the beam axis, in order to recreate conditions closer to those normally found in clinical environments. This SSSSD device with a limited number of strips and a large pitch was chosen as a first prototype for its inexpensive cost respect devices with higher spatial resolution. It was chosen for a feasibility study of the proposed technique. Measurements have been compared also with Geant4 simulations and TPS calculations for both phantom configurations. Finally a patent of this system has been proposed.

Another project was based on our experience on nuclear reactions. Following our activity related to medical applications, the Basic Nuclear Physics (FNB) group of CNA/University of Seville joined in a new collaboration dedicated to the experiment FIRST: Fragmentation of Ions Relevant for Space and Therapy [16].

Nowadays, particle therapy is an expanding field in cancer treatments, and generally exploits protons or carbon ions. Carbon ions combine significant advantages both in the physics dose-depth deposition pattern and in the biological effectiveness and may represent a significant breakthrough in hadron-therapy [17]. Nuclear fragmentation cross-sections are essential for accurate treatment planning, as only roughly 50% of the heavy ions directed to the patient actually reach a deep tumor. Treatment plans are generally based on deterministic codes, but the great accuracy ($\leq$3%) required for medical treatment planning and sparing of normal tissues surrounding the tumors makes necessary several intercomparison of the codes with Monte Carlo calculations [18]. All these calculations are based on measured nuclear fragmentation cross-sections of carbon ions in water or tissue-equivalent materials. Several measurements have been performed in the past in USA (BEVALAC and Berkeley), Japan (HIMAC in Chiba) and GSI in Germany [19]. Most of these measurements are however limited to yields or total charge-changing fragmentation cross-sections, while measurements of double-differential cross section measurements are insufficient.

From the radiation therapy viewpoint, this paper presents the characterization of a silicon strip detector for obtaining dose maps in axial plane of a cylindrical phantom, to be applied to radiotherapy treatment verification [20]. This study comprises a calibration protocol, experimental measurements, data analysis and simulations used to validate this original technique. From the particle therapy viewpoint, a brief description of the FIRST experiment performed at the SIS accelerator of GSI laboratory in Darmstadt, dedicated to the measurement of different ions fragmentation cross sections at different energies between 100 and 1000 MeV is presented.

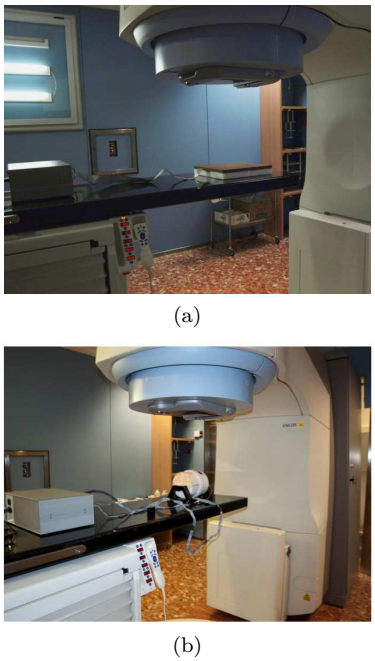

(a)

(b)

FIG. 1. PRIMUS™ linear accelerator at the Virgen Macarena University Hospital in Seville and the experimental setup with the slab phantom (a) and the cilindrical phantom (b) mounted during a test, respetively.

II. RADIATION THERAPY. EXPERIMENTAL SETUP

A Siemens PRIMUS™ linac dual energy machine operating at 6 MV photon mode has been used to irradiate and test the detection system. Two phantoms were designed to house the detector, an SSSSD, and dedicated electronics was developed. The first phantom is a $30 \times 30 \times 5$ cm^3 slab phantom made of polyethylene. Fig. 1(a) shows a picture of this experimental setup during a measurement. We can distinguish the linac and the slab phantom (with the detector inside) covered by several slices of solid water.

In addition, since in clinical practice dose distributions are customarily displayed along axial planes, a cylindrical phantom made of polyethylene (diameter of 15 cm and height of 17 cm) was used to study the behavior of the detector when it is placed parallel to the beam axis (Fig. 1(b) and 2). Such a phantom has the capability of rotating around its symmetry axis to study the angular response of the strip detector.

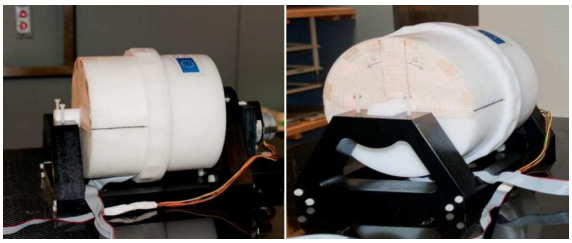

FIG. 2. The cylindrical phantom mounted during a measurement.

Software developed under LabVIEW platform enables to control the rotation of the cylindrical phantom using the RS-232 communication protocol. There are two possibilities: selecting one fixed angle or moving automatically within a set of consecutive angles. Automatic operations are integrated in the overall treatment sequence for rotating the phantom during a full treatment.

With the purpose of benchmarking this novel method, we have chosen a commercial, totally depleted, DC-coupled single-sided silicon strip detector (SSSSD), model W1(SS)-500 from Micron Semiconductor Ltd. [21]. It is 500 μm thick and is divided into 16 strips, with 3.1 mm pitch, covering an active area of 50.0×50.0 mm^2. The 16 strips consist of a region of heavily doped silicon by implantation of acceptor impurities to form a p^+ type material on a n-type silicon wafer. An aluminum metalization with a thickness of 0.3 μm is applied on the junction side allowing good ultra sonic wire bonding connections. The silicon detector is mounted on a Printed Circuit Board (PCB) frame made out of *FR4* material. The detector is connected to the readout electronics by a standard 16-conductor ribbon cable (2 m length) with an insulated displacement connector. The *W1(SS)* SSSSD design does not incorporate a guard-ring [21].

The result of the incident radiation on the silicon p-n diodes of the SSSSD is a weak current. Since we need to measure the total absorbed dose inside the material, the read-out electronics is implemented as an electrometer, thus, integrating the total received charge. The front-end electronics is a conventional charge integrator. The output voltage, proportional to the charge, is digitized by analog-to-digital converter (ADC) and analyzed using a digital signal processor (DSP). The signal is then digitally processed and transferred to a PC based application. A PC receives from the DSP a set of values. These values are written in a data array for each sampling time of the electronics. Data files present strip doses for each sampling time, at each rotation angle of the phantom, which allows a post-treatment analysis of data.

A. Geant4 simulations

The experimental setup was modeled with the Geant4 toolkit (*version 9.3.p01*) [22, 23]. The geometry of the Siemens PRIMUS™ treatment head, operating at 6 MV nominal energy photons, was reproduced in detail according to the manufacturer's specifications concerning target, flattening filter, monitor chamber, jaws and the multi-leaf collimator [24]. The geometric model of the phantoms was built according to our design layouts (including the air gaps and lateral supports) [25]. The SSSSD was also reproduced following the specifications given by the manufacturer [21]. The goal of these simulations was to estimate the sensitivity of the SSSSD in different experimental situations based on the dose in each strip. Thus, a dose deposition "scorer" was registered for each strip of the SSSSD. The Geant4 results were compared with the experimental measurements and to the calculations obtained with the TPS.

B. Experimental data: SSSSD characterization

The solid-water slab material was used to house and to characterize the detector in terms of linearity, depth dose, reproducibility, uniformity, penumbra. All the measurements were performed with a dose rate of 200 Monitor Units (MU/min). A single MU is the amount of charge measured by the ionization chamber mounted in the head of the linear accelerator, which correlates with a dose of 1 cGy delivered to a water phantom under reference conditions. The reference condition is characterized by a radiation field of 10×10 cm^2, a source-to-surface distance (SSD) equal to 100 cm and the detector placed at a depth of 1.5 cm of solid water slabs. In this configuration the absorbed dose in cGy, in the centre of the beam axis, is equal to the number of MU delivered by the linac.

The linearity of the device was determined using the raw signal (i.e. before the efficiency and gain corrections and calibration) at the output of the ADC for each electronic channel (i.e. each detector strip). This signal was registered as a function of irradiation time of the detector. As an example, the data of one single strip represented by black circles and the linear fit represented by a red line are shown in Fig. 3(a). The deviation from linearity of the dose signal in the range of 4-500 cGy is of order of 0.1%.

In order to study the reproducibility of strip signals, the detector was irradiated six times with a constant dose, under reference condition. All the strips, at different dose measurements X_i, present a reproducibility deviation better than 0.5%.

Dedicated measurements for correcting the channel to channel variation of the 16 strips were performed. These measurements were necessary since each strip of the detector and each electronic chain has a slightly different response, due to different connections, capacitance, amplifications etc. Finally, variations between all channels (strips), before applying the uniformity correction, were within 2 %. After performing the uniformity correction, the channel-to-channel variations were below 0.5 % (red closed circles of Fig. 3(b)).

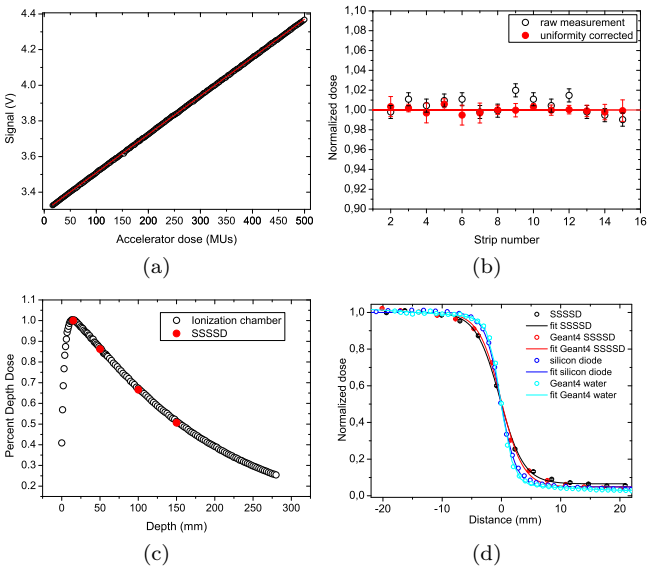

FIG. 3. (a) Measurement of the linearity of one single strip (number 11) reported with black open circles as a function of the dose delivered by the accelerator (500 MU). Red line represents a linear fit of data. (b) The raw measurement of the detector response normalized to the unit obtained with a flat field is reported with black open circles. The corrected response obtained from the uniformity factors is shown with red closed circles. (c) Dose depth curve measured with the SSSSD is reported with red closed circles and compared to the measurements performed with the ionization chamber (black open circles). (d) Penumbra measured under reference conditions. With black and red open circles the SSSSD data and Geant4 simulations (SSSSD case) are reported, respectively. With blue and cyan open circles measurements obtained with one channel silicon detector and Geant4 (dose-to-water) are shown.

Percent depth dose was also studied. The detector was housed inside the slab phantom at SSD = 100 cm. A field of 10×10 cm^2 was used to irradiate the device with 200 MU and several slabs of solid water were used to measure the percent depth dose (PDD) at the following depths: 1.5 cm, 5 cm, 10 cm and 15 cm. Fig. 3(c) shows the PDD measured by the SSSSD compared to the data of an ionization chamber. In Fig. 3(c), measurements of the SSSSD are represented with red closed circles and data of the ionization chamber with black open circles. The difference is 0.68 % at 10 cm and 0.73 % at 15 cm of depth. In all cases, the statistical errors (1σ) of the SSSSD measurements with respect to the ionization chamber are smaller than 1%.

The penumbra size of the treatment field is defined as the region between 20% and 80% of the maximum dose levels at 1.5 cm solid water depth. Half of the radiation field was blocked, defining a field of 5×10 cm^2 with the multileaf collimator (MLC). Experimental data of the SSSSD and Geant4 simulations modeling the detector are reported in Fig. 3(d) with black and red open circles, respectively. These data were compared to a measurement obtained with a one-channel silicon detector (*Scanditronix* p-Si detector) and to Geant4 simulations in a water tank, reported with blue and cyan open circles, respectively.

The penumbra obtained by the SSSSD and with the Geant4 simulation modeling the detector (SSSSD case) give a value of 6.17 ± 0.56 mm and 5.58 ± 0.25 mm, respectively. The penumbra obtained with the single channel silicon detector was 3.92 ± 0.20 mm. Finally, penumbra calculated with Geant4 in a water tank (dose-to-water) gave a value 3.84 ± 0.25 mm.

SSSSD data and Geant4 simulations (SSSSD case) are compatible within uncertainties. Data obtained with the one-channel silicon detector and with Geant4 (dose-to-water) are also compatible. However, SSSSD data gave a penumbra value larger than the one obtained when using the one-channel silicon detector and this effect is clearly visible in Fig. 3(d). This approximately 1.5 times larger penumbra for the SSSSD with respect to the one channel silicon detector is attributed to its strip pitch of 3.1 mm.

C. Angular response

Since the most common way to present dose distributions for radiotherapy is a dose map in the axial plane of the patient, as an innovation the detector was placed inside the cylindrical phantom parallel to the beam axis. A set of measurements was performed varying the gantry angle and rotating the phantom. The center of the detector, located on the rotation axis of the phantom, was positioned at the isocenter of the accelerator, located at 100 cm from the source. The phantom was irradiated with 200 MUs, using a 10×10 cm^2 radiation field. In Fig. 4 the dose deposited in each strip is shown only for four irradiation angles. For each measurement, the value of the gantry rotation angle, θ, is reported on the top of each panel. The experimental data obtained rotating the gantry and phantom are represented with red and black open circles, respectively. Fig. 4 shows a total compatibility between both experimental data described above.

A Computed Tomography (CT) image of the system in the transverse plane was performed in order to calculate the dose received by each strip with the TPS. The CT image was used to divide the active area of the device into 16 strips and the absorbed dose in each strip was calculated with the TPS (Philips Pinnacle[3]). In the TPS calculation we assumed that the entire phantom including the detector was water, so one calculates dose-to-water data. Calculated doses using the TPS are reported in Fig. 4 with blue open squares.

Geant4 simulations were performed both to estimate the dose-to-water data and for the SSSSD case. In the first case the cylindrical phantom with a density of 1 g/cm^3 (water phantom) was modeled. Geant4 simulation for the dose-to-water case is reported in Fig. 4

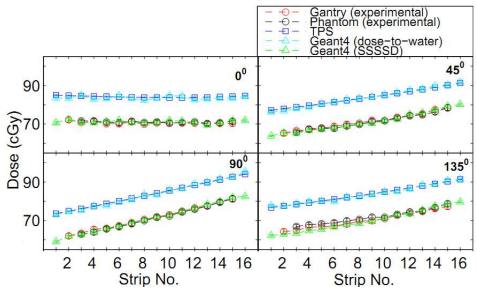

FIG. 4. Absorbed doses as function of the strip number for each angle θ of irradiation. Experimental data rotating the gantry and phantom are reported with red and black open circles, respectively. TPS data are reported with blue open squares. Geant4 simulations (dose-to-water case) and Geant4 (SSSSD case) are reported with cyan and green open triangles, respectively.

with cyan open triangles. The latter simulation is fully compatible with TPS calculations. The relative difference between these data is smaller than 1.7 % for all the strips at different angle orientations. Geant4 simulation for the SSSSD case is also reported in Fig. 4 with green open triangles. Simulations are compatible with the experimental data measured with the SSSSD. Small differences are due to the alignment and to the errors in the angle of rotation of the detector inside the cylindrical phantom.

In Fig. 4 differences of about 14 % between calculations obtained using the TPS and the SSSSD data are evident. These differences can be attributed to the different orientations of the detector: in the cylindrical phantom (parallel configuration) and in the slab phantom (perpendicular configuration), in which the dose calibration was obtained. Consequently a new calibration factor is necessary for the parallel configuration.

In order to study the quantitative differences between TPS and experimental data and to investigate the dependence of the dose with respect to the strip number "i" and the irradiation angle θ, ratios $K_i(\theta)$ between SSSSD doses D_i and TPS doses D_i^{TPS} were calculated for each strip: $K_i(\theta) = D_i(\theta)/D_i^{TPS}(\theta)$. The ratio between experimental data and TPS at different angles was constant within error bars. From these results, for each strip we found a calibration factor $K_i(\theta)$ independent of the irradiation angle $K_i(\theta) \approx K_i$. The non dependence on the irradiation angles with respect to the strips is a remarkable result that simplifies outstandingly the detector calibration.

Finally, calibrated doses D^{cal} with respect to the TPS were calculated by dividing the measured dose D_i by the K_i factors from this equation, $D_i^{cal} = D_i/K_i$ and compared to the TPS calculations and Geant4 simulations (dose-to-water case). The relative difference between the calibrated dose and TPS calculations was found better than 2 % for the strips at the edges of the SSSSD, and even better than 1 % for the central ones.

III. PARTICLE THERAPY: FIRST EXPERIMENT AT GSI

A new project was dedicated to study fragmentation processes relevant on hadron-therapy, with the participation in the experiment named FIRST: Fragmentation of Ions Relevant for Space and Therapy carried out at GSI. The scientific program of the FIRST experiment was focused on the study of the 400 MeV/nucleon ^{12}C beam fragmentation on thin (5mm) graphite target. The experiment was performed by an international collaboration made of institutions from Germany, France, Italy and Spain.

The experiment FIRST consists of several subdetectors, divided in two main blocks: the interaction region and the large detector region. A schematic view of the experiment is reported in Fig. 5.

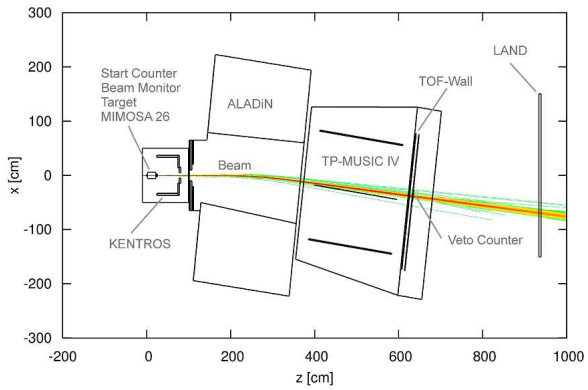

FIG. 5. A top view of the experiment FIRST. The red line in the middle represent the position of the beam.

The two regions are very different in dimensions of the corresponding detectors: impinging beam and produced fragments are studied in the IR within some tens of centimeters from the target, while the devices that detect the fragments, after magnetic bending, in the large detector region have typical dimension of meters. Following the beam path, the interaction region is made of a Start Counter (SC) scintillator that provides the start to the Time Of Flight measurement, a drift chamber Beam Monitor (BM) that measures the beam trajectory and impact point on the target, a robotized target system, a pixel silicon Vertex Detector (VD) to track the charged fragments emerging from the thin target and a thick scintillator Proton Tagger (PT) that detects the light fragments at large angles. Due to the reduced dimension, all the interaction region is in air. This choice greatly helps the design and the running of the interaction region (IR) detectors, increasing the out of target interaction proba-

bility only by 5%. With the noticeable exception of the large angle protons and a little fraction of ^{4}He, most of the projectile fragments are produced in the forward direction with the same β of the beam. These fragments are then in the magnetic acceptance of the ALADIN dipole magnet and after magnetic bending they enter in the large detector region. A large area system of scintillators (ToF-WALL) provides the measurement of the impinging point and the arrival time of the particles. In correspondence of the non interacting beam path, after the ToF-WALL, a scintillator sandwich detector (Veto Counter) analyzes the carbon beam. Finally the Large Area Neutron Detector (LAND2), made of a stack of scintillator counters, gives information about the neutrons emitted within an angle of 10 deg with respect to the beam.

Following DITANET objectives and requirements, the work was dedicated to the reconstruction software of the experiment, both for the beam tracking reconstruction of the fragments using Monte Carlo simulations of the experiment as for the reconstruction software of the beam monitor drift chamber, used to measure the beam trajectory and the impact point on the target with a resolution of 100 μm. Experimental data have been carried out during Summer 2011 and the analysis of the data is in progress.

IV. CONCLUSIONS

Radiation and particle therapy are techniques widely used in cancer treatments and in continuous progress. The described project aimed to contribute to this process, with the main objective of applying the background of the CNA/University of Seville in particle reactions and nuclear instruments, following DITANET requirements, to therapy research and treatments. The work on this field was developed during the DITANET Experienced Researcher contract from 2008 to 2011, based on a local research project/collaboration named RADIA2, which was dedicated to study the feasibility of using silicon strip detectors for complex radiotherapy treatments verifications. The project joined a local collaboration between the CNA, the Department of Atomic, Molecular and Nuclear Physics (FAMN), the Superior Engineering School and the Virgin Macarena Hospital of the University of Seville and the private company Inabensa S. A. During this project, the collaboration studied the use of a silicon strip detector with its electronics, to develop a mechanical setup and an acquisition software, for obtaining radiation dose maps with an in-house reconstruction algorithm. Phantoms were used to simulate the human body and to adapt detectors to clinical conditions. Detectors were irradiated by 6 MV linac available at the University Hospital. The treatment head of the linac, phantoms and detector were modelled with the Geant4 toolkit. Thus, experimental doses were compared to powerful Monte Carlo simulations and to the Treatment Planning System (TPS) calculations of the hospital. The feasibility study comprised a calibration protocol, the designed experimental set-up, measurements, data analysis and simulations. In addition, it was possible to study the angular response of the detector, and more importantly, to obtain dose maps in axial planes, which are valuable for complex radiation therapy treatment verification. As a main result, an original technique has been validated and is in the process of being patented.

The background of CNA in particle reactions and instruments added to medical applications interests, developed by certain projects, guided this research also to the particle therapy field. With the aim of linking radiation and particle therapy, the USE/CNA took part into the FIRST (Fragments and Ions Relevant for Space and Therapy) international collaboration, for measuring and analysing nuclear fragmentation cross-sections essential for accurate particle treatment planning. In the FIRST collaboration, we work in the data taking and in the beam tracking reconstruction of the detected fragments, using Monte Carlo simulations of the experimental setup as well as in the reconstruction software for the beam monitor drift chamber, in order to measure the beam trajectory and the impact point on the target with resolutions of order of 100 μm.

[1] C. D. Wagter, Journal of Physics: Conference Series **3**, 4 (2004).

[2] E. B. Podgorsak, ed., *Radiation Oncology Physics: A Handbook for Teachers and Students* (IAEA, Available online from www.iaea.org, 2005).

[3] IMRT Collaborative Working Group, International Journal of Radiation Oncology Biology Physics **51**, 880 (2001).

[4] J. Dyk, R. Barnett, J. Cygler, and P. Shragge, Int. J. Radiat. Oncol. Biol. Phys. **26**, 261 (1993).

[5] P. Cadman, R. Bassalow, N. Sidhu, G. Ibbott, and A. Nelson, Physics in Medicine and Biology **47**, 3001 (2002).

[6] M. Bucciolini, F. B. Buonamici, and M. Casati, Medical Physics **31**, 161 (2004).

[7] F. Banci Buonamici and et al., Medical Physics **34**, 1372 (2007).

[8] J. Li, G. Yan, and C. Liu, Journal of Applied Clinical Medical Physics **10**, 62 (2009).

[9] S. Saminathan, R. Manickam, V. Chandraraj, and S. Supe, Journal of Applied Clinical Medical Physics **11** (2010).

[10] R. Ballabriga, M. Campbell, E. Heijne, X. Llopart, L. Tlustos, and W. Wong, NIM-a **633, 1**, S15 (2010).

[11] J. H. D. Wong, M. Carolan, M. L. F. Lerch, M. Petasecca, S. Khanna, V. L. Perevertaylo, P. Metcalfe, and A. B. Rosenfeld, Medical Physics **37**, 427 (2010).

[12] I. Redondo-Fernandez, C. Buttar, S. Walsh,

S. Manolopoulos, J. Homer, S. Young, and J. Conway, *Proceedings of the 7th International Conference on Position-Sensitive Detectors - PSD-7, 7th International Conference on Position-Sensitive Detectors*, NIM-a **573**, 141 (2007).

[13] C. Talamonti, M. Bruzzi, M. Bucciolini, L. Marrazzo, and D. Menichelli, *Proceedings of the 6th International Conference on Radiation Effects on Semiconductor Materials, Detectors and Devices - RESMDD 2006*, NIM-a **583**, 114 (2007).

[14] S. Manolopoulos, C. Wojnecki, R. Hugtenburg, M. A. J. Sidek, G. Chalmers, G. Heyes, and S. Green, Physics in Medicine and Biology **54**, 485 (2009).

[15] D. Menichelli, M. Bruzzi, M. Bucciolini, C. Talamonti, M. Casati, L. Marrazzo, M. Tesi, C. Piemonte, A. Pozza, N. Zorzi, M. Brianzi, and A. De Sio, *Proc. of RESMDD 2006*, NIM-a **583**, 109 (2007).

[16] R. Pleskac, Z. Abou-Haidar, C. Agodi, M. Alvarez, T. Aumann, G. Battistoni, A. Bocci, T. Bhlen, A. Boudard, A. Brunetti, M. Carpinelli, G. Cirrone, M. Cortes-Giraldo, G. Cuttone, M. De Napoli, M. Durante, J. Fernndez-Garca, C. Finck, B. Golosio, M. Gallardo, E. Iarocci, F. Iazzi, G. Ickert, R. Introzzi, D. Juliani, J. Krimmer, N. Kurz, M. Labalme, Y. Leifels, A. Le Fevre, S. Leray, F. Marchetto, V. Monaco, M. Morone, P. Oliva, A. Paoloni, L. Piersanti, J. Quesada, G. Raciti, N. Randazzo, F. Romano, D. Rossi, M. Rousseau, R. Sacchi, P. Sala, A. Sarti, C. Scheidenberger, C. Schuy, A. Sciubba, C. Sfienti, H. Simon, V. Sipala, E. Spiriti, L. Stuttge, S. Tropea, H. Younis, and V. Patera, Nuclear Instruments and Methods in Physics Research Section A: Accelerators, Spectrometers, Detectors and Associated Equipment **678**, 130 (2012).

[17] O. Jkel, C. P. Karger, and J. Debus, Medical Physics **35**, 5653 (2008).

[18] T. T. Bhlen, F. Cerutti, M. Dosanjh, A. Ferrari, I. Gudowska, A. Mairani, and J. M. Quesada, Physics in Medicine and Biology **55**, 5833 (2010).

[19] D. Schardt, T. Elsässer, and D. Schulz-Ertner, Rev. Mod. Phys. **82**, 383 (2010).

[20] A. Bocci, M. Cortes-Giraldo, M. Gallardo, J. Espino, R. Arrans, M. Alvarez, Z. Abou-Haidar, J. Quesada, A. Perez Vega-Leal, and F. Perez Nieto, Nuclear Instruments and Methods in Physics Research Section A: Accelerators, Spectrometers, Detectors and Associated Equipment **673**, 98 (2012).

[21] (http://www.micronsemiconductor.co.uk/).

[22] S. Agostinelli and et al., NIM-a **506**, 250 (2003).

[23] J. Allison and et al., IEEE Transactions on Nuclear Science **53**, 270 (2006).

[24] M. A. Cortes-Giraldo, J. M. Quesada, and M. I. Gallardo, AIP Conference Proceedings **1231**, 209 (2010).

[25] M. A. Cortes-Giraldo, M. I. Gallardo, R. Arrans, J. M. Quesada, A. Bocci, J. M. Espino, Z. Abou-Haidar, and M. A. G. Alvarez, *Proc. of SNA-MC-2010 Conference*, Progress in Nuclear Science and Technology, in press (2010).